

Power Stability Analysis of a Meshed MMC-MTDC Link with Voltage Margin Control

Maxwel da S. Santos* Flavio B. Costa** Luciano S. Barros***
Luana C. S. Soares**** Camila M. V. Barros***

* *Postgraduate Program in Electrical and of Computer Engineering,
Federal University of Rio Grande do Norte, Natal-RN, Brazil, (e-mail:
maxwel@ufrn.edu.br).*

** *Electrical and Computer Engineering Department, Michigan
Technological University, Michigan, USA (e-mail: fbcosta@mtu.edu)*

*** *Computer Systems Department, Federal University of Paraíba, João
Pessoa-PB, Brazil, (e-mail: lsalesbarros@ci.ufpb.br,
camila.barros@ci.ufpb.br)*

**** *Postgraduate Program in Electrical Engineering, Federal
University of Paraíba, João Pessoa-PB, Brazil, (e-mail:
luana.soares@cear.ufpb.br)*

Abstract: In modern power systems, transmission over long distances and offshore wind energy conversion systems increasingly use the technology of high voltage direct current transmission due to cheaper investment costs, lower power losses, and better controllability. However, effective integration of this technology drastically reduces the overall system's inertia. This paper proposes a stability analysis of a meshed multi-terminal high voltage direct current (MTDC) system based on modular multilevel converter (MMC) with voltage margin control to connect four distinct AC grids. Simulations assessed the system performance to remain stable under abnormal operating conditions in the AC grids, such as load variations. Results suggest although a disturbance in an AC grid does not cause variations in other AC grids due to the MTDC link, it can generate variations in the DC grid.

Resumo: Nos sistemas de energia modernos, a transmissão em longas distâncias e os sistemas de conversão de energia eólica offshore usam cada vez mais a tecnologia de transmissão de corrente contínua de alta tensão devido aos custos de investimento mais baratos, menores perdas de energia e melhor controlabilidade. No entanto, a integração efetiva dessa tecnologia reduz drasticamente a inércia geral do sistema. Este trabalho propõe uma análise de estabilidade de um sistema de corrente contínua de alta tensão multiterminal (MCCAT) em malha baseado em conversor multinível modular (CMM) com controle de margem de tensão para conectar quatro redes CA distintas. As simulações avaliaram o desempenho do sistema para permanecer estável sob condições anormais de operação nas redes CA, como variações de carga. Os resultados sugerem que embora uma perturbação em uma rede CA não cause variações em outras redes CA devido ao link MCCAT, pode gerar variações na rede CC.

Keywords: Modular multilevel converter, multi-terminal high voltage direct current systems, power system stability, synchronous generation, voltage margin control.

Palavras-chaves: Controle de margem de tensão, conversor multinível modular, estabilidade do sistema de energia, geração síncrona, sistemas de corrente contínua de alta tensão multiterminal.

1. INTRODUCTION

The electricity demand is increasingly intense worldwide, especially in technological and industrial development countries. Usually, this demand occurs in regions very distant from existing generation centers (Pfeiffer et al., 2018). In this scenario, the discussion arises on how to transmit large energy blocks more efficiently.

The high voltage direct current (HVDC) transmission is the best alternative for electric energy transmission over long distances. This is because the HVDC lines have neither reactive losses nor skin effect, i.e., the lines suffer minor losses and have smaller diameters, which reduces their cost (Sanchez et al., 2019). In addition, HVDC can also connect asynchronous AC grids.

The HVDC links can be classified as point-to-point links if connected between two points of a single AC system or two separate AC systems, or multi-terminal high voltage direct current (MTDC) links when there are more than

* This work was supported by the National Council for Scientific and Technological (CNPq) and by the Coordination for the Improvement of Higher Education Personnel (CAPES), Brazil.

two points of connections to the AC system. The use of an MTDC grid rather than multiple point-to-point links lies in their advantages of system integrated operation (Ye et al., 2021). The MTDC link can reroute its power flows when a failure or a maintenance occurs in the DC grid. As a result, its peak demand is much less than the sum of peak demands of multiple point-to-point links. It also reduces the spinning reserve requirement in synchronous generations (Ye et al., 2021).

A modular multilevel converter (MMC) is the best option among the MTDC transmission technologies based on voltage source converters (VSCs) (Du et al., 2018). This technology presents the capability to control active and reactive power independently, reduced output filters due to low harmonic distortion, low switching losses, and better fault performance (Du et al., 2018).

Power system stability is the ability to remain in operating equilibrium after suffering a disturbance (Alves et al., 2021). Therefore, power system stability analysis consists of rotor angle stability, frequency stability, and voltage stability (Machowski et al., 2020). Thus, the power system stability consists of the balance between generated and consumed power.

A conventional electrical power system (EPS) consists of synchronous generators (SG) and passive elements connected to form an extensive system (Machowski et al., 2020). In the EPS, the power variation supplied by the SGs is not delivered instantly, i.e., it provides power smoothly without exerting sudden changes in voltage and frequency in the coupling point (Alves et al., 2021). Thus, the SGs inherently contribute to the maintenance of power stability by increasing the EPS overall inertia. On the other hand, the HVDC links do not inherently contribute to the system inertia due to the fast power reference control of the converters. Moreover, the HVDC links and distributed generation (DG) based on asynchronous frequency sources are likely to integrate a significant fraction of the EPS in the future, drastically reducing the EPS overall inertia.

This paper proposes an analysis of a four-terminal MMC-MTDC system with meshed topology to connect four distinct AC grids. The converter stations control system used is the voltage margin control strategy. Simulation assessed the system's performance in an MMC-MTDC link under abnormal operating conditions in the AC grids. The AC grids comprise a hydroelectric power plant (HPP) with a power governor and automatic voltage regulator (AVR) with power system stabilizer (PSS), AC transmission lines, power transformers, and loads. The operation scenario considers a challenging and common failure for power system stability, such as load variations in the AC grids connected from an MMC-MTDC system.

2. MULTI-TERMINAL HIGH VOLTAGE DIRECT CURRENT

This section presents the MTDC grid topology used and its controls. The main purpose of the MTDC grid is to share the power flow between its terminals.

2.1 MTDC Topology

Based on Leterme et al. (2015), Fig. 1 depicts the used MTDC grid. The system topology is a meshed DC grid with five monopolar cables with metal returns. The cables connect the four converter stations based on MMCs to each other. Each DC line terminal presents current limiting reactors (L_r), and each converter has 101 levels.

In a meshed-connected MTDC link, at least two converter stations have more than one DC connection. These links may establish a parallel path for the power flow between the terminals. The parallel links introduce redundancy to the transmission links and increase the system's reliability and availability (Chaudhuri et al., 2014). Thus, the DC-bus voltages and transmission lines resistances determine the currents of the DC lines.

2.2 Converter Control System

The voltage margin control scheme has the purpose of sharing the responsibility for regulating the DC voltage among two or more terminals (Du et al., 2018; Santos et al., 2022b). The master converter station is responsible for the voltage regulation of the DC grid. This converter station is also called a slack bus and works in constant voltage control mode. The remaining converters, named slave stations, are responsible for the power flow regulation of the grid and work in the constant power control mode (Rekik et al., 2018). This control strategy can also transfer the slack bus function to the backup converter station in case of an outage of the main slack bus (Santos et al., 2022b). When the DC voltage is within the upper and lower limits, the backup slack bus work in the constant power control mode. On the other hand, when the DC voltage exceeds either the upper or the lower limits, it will work into the constant voltage control mode.

Fig. 2 shows the voltage margin control blocks. It consists of two control meshes: inner and outer loops. The internal control loop regulates the converter currents, whereas the external control regulates the DC voltage or power flow. The outer control loop is decentralized, which implies that each converter station operates based only on local information.

The connection of converter with the AC grid is made through an equivalent three-phase impedance RL . Applying the inverse Clarke transformation, for $\theta = \theta_g$, where θ_g is the AC grid voltage angle obtained through a phase-lag locker loop (PLL), the grid-connection dq model is given by (Santos and Barros, 2019):

$$v_d^g = R_{arm}i_d^g + L_{arm}\frac{d i_d^g}{dt} - \omega_g L_{arm}i_q^g + V_g \quad (1)$$

and

$$v_q^g = R_{arm}i_q^g + L_{arm}\frac{d i_q^g}{dt} - \omega_g L_{arm}i_d^g, \quad (2)$$

where v_d^g and v_q^g are voltages in dq frame at the output of the converter; i_d^g and i_q^g are currents in dq frame at the impedance of the converter; ω_g is the grid frequency; V_g

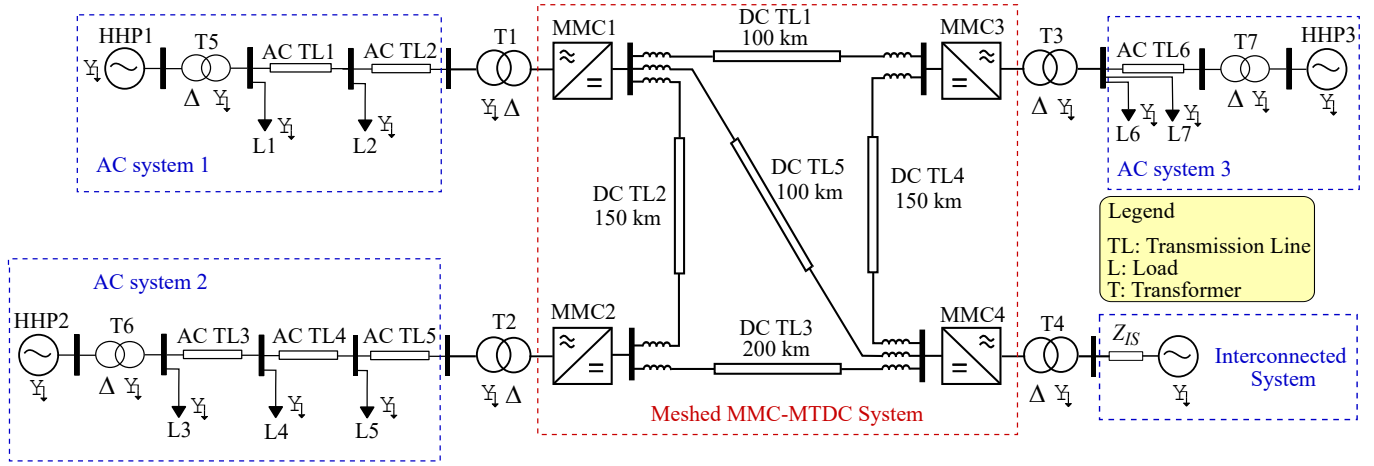


Fig. 1. Single line diagram of the meshed MMC-MTDC system.

is the grid voltage; $\omega_g L_{arm} i_q$ (e_{sd}) and $\omega_g L_{arm} i_d$ (e_{sq}) are the cross coupling terms.

In the θ_g reference, the active and reactive power delivered to the AC grid are given by (Santos and Barros, 2019):

$$P_g = V_g i_d^g \quad (3)$$

and

$$Q_g = -V_g i_q^g. \quad (4)$$

Thus, the active and reactive power can be controlled, respectively, with components of the direct axis (i_d) and quadrature axis (i_q) of the current delivered to the AC grid. The constant power control scheme includes a PI controller ensures that the power delivered to the DC side is maintained at P_g^* .

The DC-bus voltage (V_{dc}) is obtained as follows:

$$C \frac{dV_{dc}}{dt} = i_c = \frac{P_{dc} - P_g}{V_{dc}}, \quad (5)$$

where C is the equivalent capacitance of the DC-bus; i_c is the current of the DC-bus; P_{dc} is the power from the DC grid; P_g is the output power of the converter.

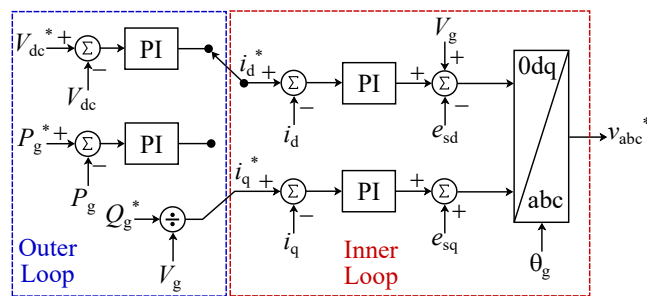


Fig. 2. Voltage margin control strategy.

3. MODULAR MULTILEVEL CONVERTER

Fig. 3 depicts the MMC used in this work. Its legs number is equal to the phases number of the AC grid. Each leg is formed into two arms, which are composed of N SMs and an arm inductor L_{arm} connected in series. The L_{arm} main purpose is to limit the high-frequency currents resulting from the difference between the instant voltages generated by the arms. The arm resistor R_{arm} represents the equivalent of the sum of the conduction resistance of the SMs and ohmic losses of the arm circuit. Each SM contains a half-bridge of two insulated gates bipolar transistors (IGBTs) and a capacitor C_{sm} .

3.1 Phase Disposition Pulse Width Modulation

The Phase-disposition pulse width modulation (PD-PWM) is a scalar pulse width modulation adapted for use in the multilevel converters (Martinez-Rodrigo et al., 2017). It belongs to the high switching frequency modulation category ($f_{sw} \geq 2$ kHz). A low-frequency modulator signal is compared with triangle carrier signals to produce the output voltage in this modulation.

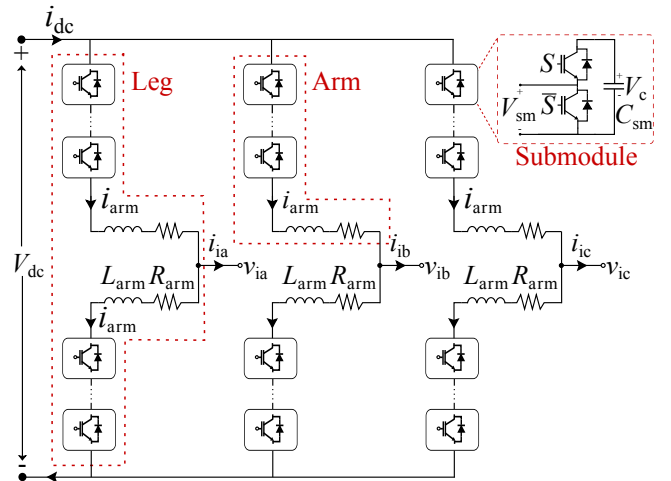


Fig. 3. The used MMC.

3.2 Capacitor Balancing Algorithm

The SMs capacitor voltages vary depending on the current flowing through them. However, the objective is to keep the capacitor voltages approximately equal to their nominal value, V_{dc}/N , for the flawless operation of MMC (Martinez-Rodrigo et al., 2017). The capacitor balancing algorithm (CBA) performs the capacitor voltages balancing of SMs. For this, it measures the capacitor voltages and chooses the SM to be ON according to the own arm's current direction, i_{arm} (Geng et al., 2022). When i_{arm} is positive, i.e., when the current flows from the DC grid to the AC grid, the SMs with the lowest voltage values are turned ON to charge their capacitors. Conversely, when i_{arm} is opposing, the SMs with the highest voltage values are turned ON to discharge their capacitors.

4. HYDROELECTRIC POWER PLANT

Fig. 4 depicts the HPP model with speed regulator, AVR, and PSS. The hydraulic turbine is fixed blade type (Kundur, 1994). The Appendix presents the HPP parameters.

4.1 Hydraulic Turbine

Assuming a rigid conduit and incompressible fluid, the velocity of the water in the penstock, the mechanical power of the hydraulic turbine, and the acceleration of the water column due to a change in the head at the turbine are given by (Kundur, 1994):

$$U = K_u G \sqrt{H}, \quad (6)$$

$$P_m = A \rho g (UH), \quad (7)$$

and

$$\frac{dU}{dt} = -\frac{g}{L}(H - H_o), \quad (8)$$

where U is the water velocity, K_u is a constant of proportionality, G is the gate position, H is the hydraulic head at the gate, P_m the mechanical power of the hydraulic turbine, A is the pipe area, ρ is the mass density, g the gravity acceleration constant, L the length of conduit, and H_o is the initial steady-state value of H .

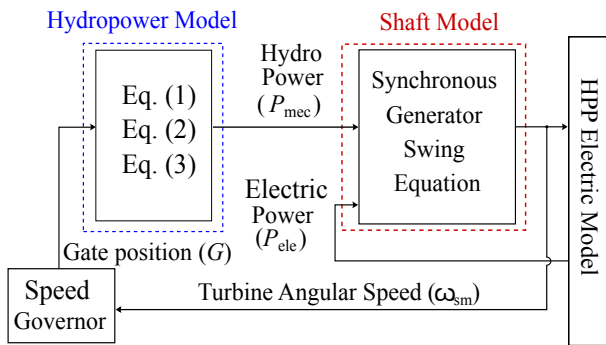


Fig. 4. HPP model with speed regulator, AVR, and PSS.

The governor of the hydraulic turbine is responsible for extracted power. Its function is to control the speed of the turbine through the control of the gate position.

The synchronous machine model is the classic with an excitation system and PSS. In this model, the mechanical angle varies according to the required electrical power of the synchronous machine according to (Kundur, 1994):

$$\frac{d^2\theta_{sm}}{dt^2} = \frac{1}{J_{sm}}(T_{mec} - T_{ele}), \quad (9)$$

4.2 Exciter and Power Stabilizer Systems

Fig. 5 depicts the excitation system with PSS model. It is a simplified representation of thyristor excitation systems classified as type ST1A. The essential function of a PSS is to add damping to the generator rotor oscillations by controlling its excitation using auxiliary stabilizing signals.

In Fig. 5, E_t is the generator terminal voltage, T_R represents the terminal voltage transducer time constant, K_A is the exciter gain, E_{fd} is the generator field voltage, K_{STAB} is the stabilizer gain, T_W represents the washout high-pass filter time constant, and T_1 and T_2 represents the phase compensation time constants.

5. PERFORMANCE ASSESSMENT

Fig. 1 depicts the used MTDC system. There are five monopolar cables with current limiting reactors (L_r). On the AC side, the AC system 1 connected in the MMC1 consists of a hydroelectric power plant (HPP) with a power governor, two AC transmission lines, two power transformers, and two loads. The AC system 2, connected to the MMC2, consists of an HPP with a power governor, three AC transmission lines, two three-phase power transformers, and two three-phase loads. The AC system 3, connected to the MMC3, consists of an HPP with a power governor, one AC transmission line, a three-phase transformer, and one three-phase load. The AC system connected to the MMC4 consists of an ideal AC source in series with a RL equivalent impedance. The AC line model is the π -nominal; the load model is the constant impedance, and the transformer model is the delta-grounded wye step-down connection. The HPP model and their control, AC line model, the load model, and transformer model are given in (Santos et al., 2022a). The Appendix presents the parameters of the MTDC system and the AC transmission lines.

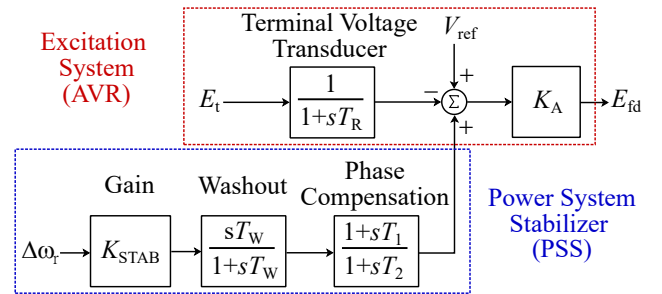


Fig. 5. AVR/exciter system with PSS model.

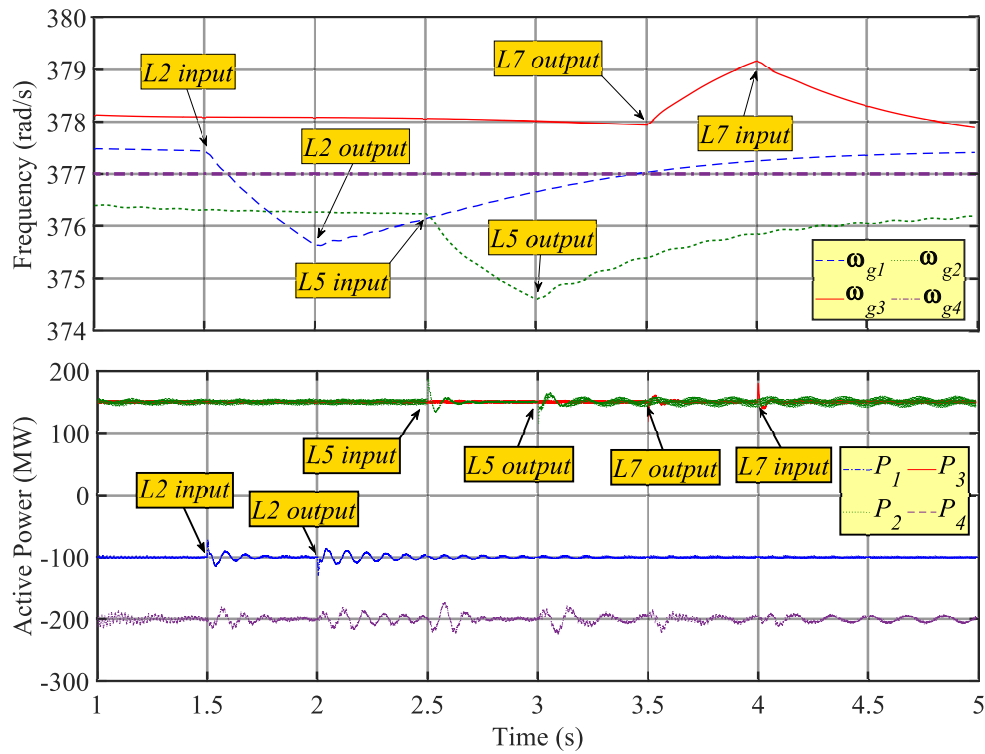


Fig. 6. Frequencies and active power flows of the meshed MMC-MTDC system with voltage margin strategy operating during load variations in the AC grids.

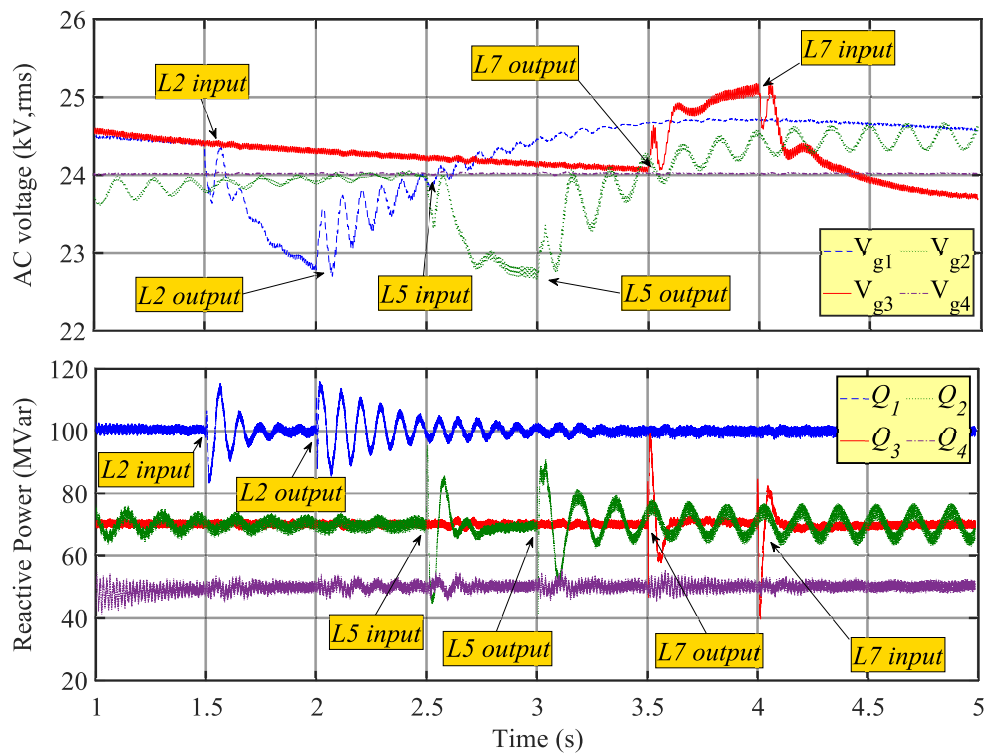


Fig. 7. AC voltages and reactive power flows of the meshed MMC-MTDC system with voltage margin strategy operating during load variations in the AC grids.

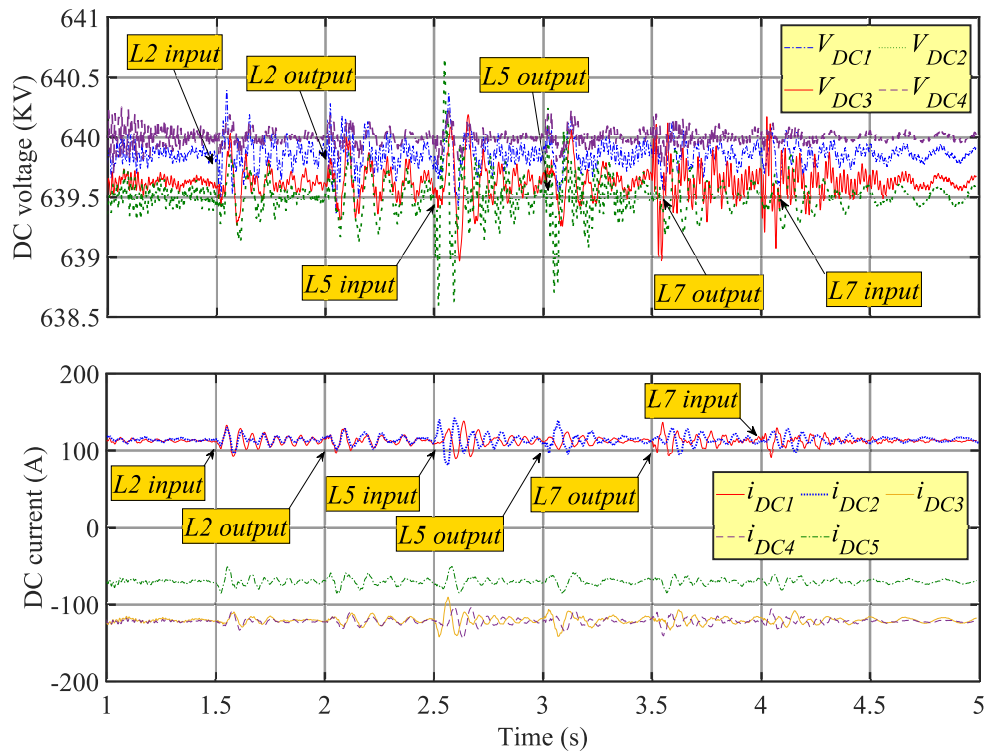


Fig. 8. DC voltages and currents of the meshed MMC-MTDC system with voltage margin strategy operating during load variations in the AC grids.

Comparative performance analyzes were carried out through simulations of the MMC-MTDC system with the voltage margin strategy operating during load variations in the AC grids. Initially, the MTDC system operates in a steady-state, in which MMC1, MMC2, MMC3, and MMC4 deliver -100 MW, 150 MW, 150 MW, and -200 MW active power flow and 100 MVar, 70 MVar, 70 MVar, and 50 MVar reactive power flow, respectively. In 1.5 and 2.0 s, the input and output of the load L2 occur, respectively, causing variations in the frequency and voltage of the AC grid 01. In 2.5 and 3.0 s, the input and output of the load L5 occur, respectively, causing variations in the frequency and voltage of the AC grid 02. Finally, in 3.5 and 4.0 s, the output and input of the load L7 occur, respectively, causing variations in the frequency and voltage of the AC grid 03. The frequency and voltage variations arise due to the power imbalance in the AC grids. This scenario considers challenging and common failures events for the AC grids.

Figs. 6 to 8 depicts the frequency, active power flows of the MMCs, AC voltages, reactive power provided by MMCs, DC-bus voltages, and currents in the DC lines of the meshed MMC-MTDC system under load variations of the 20% in the AC grids. The load variation in L2 of AC grid 01 causes a frequency variation in ω_{g1} from 377.4 rad/s to 375.6 rad/s, i.e., about -0.51%, and a voltage variation in V_{g1} from 24.5 kV to 22.8 kV, i.e., about -6.90%. The L2 variation does not cause variations in other AC grids of the MTDC link. The load variation in L5 of AC grid 02 causes a frequency variation in ω_{g2} from 376.4 rad/s to 374.6 rad/s, i.e., about -0.52%, and a voltage variation in V_{g2} from 24.0 kV to 22.8 kV, i.e., about -5.01%. The L5 variation does not cause variations in other AC grids

of the MTDC link. The load variation in L7 of AC grid 03 causes a frequency variation in ω_{g3} from 378.1 rad/s to 379.2 rad/s, i.e., about +0.33%, and a voltage variation in V_{g3} from 24.1 kV to 25.1 kV, i.e., about +4.02%. The L7 variation also does not cause variations in other AC grids of the MTDC link.

The frequency and AC voltage remained operating within stability limits of $\pm 1\%$ for frequency and $\pm 5\%$ for voltage during the load variations of $\pm 20\%$ in L2, L5, and L7. However, for load variation bigger than the studied case, the system stability can be compromised. Table 1 depicts the frequency and magnitude voltage deviations for different magnitudes of load variation. The AC grids 01, 02, and 03 do not maintain the power system stability for load variations greater than 30% in L2, L5, and L7, respectively.

The load variations, although not causing variations in other AC grids, cause variations in the MTDC link. In the active and reactive power flows, it causes variations that can reach 12.5% and 35.8%, respectively. In DC-bus voltage, it causes variations that can reach 0.2%. In the DC line currents, it causes variations of about

Table 1. Simulations of load variations.

Load Variation	$\Delta\omega_{g1}$ (%)	$\Delta\omega_{g2}$ (%)	$\Delta\omega_{g3}$ (%)	ΔV_{g1} (%)	ΔV_{g2} (%)	ΔV_{g3} (%)
$\pm 15\%$	-0.35	-0.37	+0.22	-5.02	-3.63	+3.01
$\pm 20\%$	-0.51	-0.52	+0.33	-6.90	-5.01	+4.02
$\pm 25\%$	-0.62	-0.73	+0.65	-7.51	-7.75	+8.32
$\pm 30\%$	-0.81	-0.92	+0.84	-8.01	-9.22	+9.02

20.0%. However, it can keep operating in equilibrium after suffering a disturbance until it stabilizes.

The converters of the MTDC link with voltage margin control behave like a constant power source, i.e., under operation during disturbances, it tends to keep their constant power flow. Therefore, these systems do not contribute to the AC grid to remain operating in equilibrium after suffering disorders. Thus, novel control strategies and methods based on modifications in the existing control systems of these systems are studied and proposed to help solve the overall system's inertia.

6. CONCLUSIONS

This paper performs a stability analysis of a meshed multi-terminal high voltage direct current system based on the modular multilevel converter with voltage margin control to connect four distinct AC grids. The operation scenario considered load variations in the AC grids of the MTDC link.

For the study case, the load variations in the AC grid do not caused variations in other AC grids. Therefore, the other AC grids operate without suffering frequency and voltage deviations during the disturbance. In the AC grid where the disturbance occurs, the frequency and AC voltage remained operating within stability limits during the load variations of 20%. However, more severe load variations can compromise the power system stability. Thus, each AC grid can not maintain its power system stability for load variations bigger than 30% in their load. Furthermore, the load variations caused variations in the active and reactive power flows, DC-bus voltage, and DC line currents of the MTDC link. However, the system has stabilized and continued operating in equilibrium after suffering a disturbance.

In the MTDC links, the classical control systems focus only on the DC grid, i.e., these systems do not contribute to the power stability of the AC grids.

7. APPENDIX

Table 2 summarizes the MTDC system parameter data (Leterme et al., 2015). The parameter data of the AC transmission lines and the HPP (Santos et al., 2022a) are presented in Tables 3 and 4, respectively. Table 5 summarizes the MTDC control systems parameters (Santos et al., 2022b).

Table 2. MTDC system parameters.

Parameters	Value	Unit
DC-bus voltage V_{dc}	640	kV
AC voltage V_{ac}	370	kV
MMC arm inductance L_{arm}	50	mH
MMC arm resistance R_{arm}	0.1	Ω
MMC submodule capacitance C_{sm}	10	mF
DC resistance cable R_{dc}	10	m Ω
Current limiting reactor L_r	10	mH

Table 3. AC transmission lines and loads parameters.

Element	R (Ω)	X (Ω)	C (nF)	P (MW)	Q (MVar)
TL1	5.68	13.78	22.82	-	-
TL2	16.93	40.73	0.05	-	-
TL3	5.68	13.78	22.82	-	-
TL4	18.84	27.75	37.51	-	-
TL5	16.93	40.73	0.05	-	-
TL6	22.61	54.51	22.86	-	-
L1	-	-	-	255.7	169.4
L2	-	-	-	51.14	33.88
L3	-	-	-	147.3	58.2
L4	-	-	-	255.7	169.4
L5	-	-	-	80.60	45.52
L6	-	-	-	260.7	172.7
L7	-	-	-	65.17	43.18

Table 4. HPP parameters.

Parameters	Value	Unit
P	555	MVA
V	24	kV
H_r	165	m
V_{fluid}	7.62	m/s
A	44.15	m ²
l	300	m
J_{sm}	27530	kg/m ²
L_{sm}	27.53	μ H

Table 5. MTDC control system parameters.

Parameters	K_p	K_i
Inner current control loop	500	5e3
Outer power control loop	0.2	80
Outer DC voltage control loop	-0.1	-1.2

ACKNOWLEDGMENT

This work was supported by the National Council for Scientific and Technological (CNPq) and by the Coordination for the Improvement of Higher Education Personnel (CAPES), Brazil.

REFERENCES

- Alves, E., Bergna-Diaz, G., Brandao, D., and Tedeschi, E. (2021). Sufficient conditions for robust frequency stability of ac power systems. *IEEE Transactions on Power Systems*, 36(3), 2684–2692.
- Chaudhuri, N.R., Chaudhuri, B., Majumder, R., and Yazdani, A. (2014). *Multi-Terminal Direct-Current Grids: Modeling, Analysis, and Control*. John Wiley, Hoboken, NJ, USA, 1 edition.
- Du, S., Dekka, A., Wu, B., and Zargari, N. (2018). *Modular Multilevel Converters: Analysis, Control, and Applications*. John Wiley, Hoboken, NJ, USA, 1 edition.
- Geng, Z., Han, M., Xia, C., and Kou, L. (2022). A switching times reassignment-based voltage balancing strategy for submodule capacitors in modular multilevel hvdc converters. *IEEE Transactions on Power Delivery*, 37(2), 1215–1225.
- Kundur, P. (1994). *Power System Stability and Control*. McGraw-Hill, New York, USA, 1 edition.

- Leterme, W., Ahmed, N., Beerten, J., Ängquist, L., Hertem, D.V., and Norrga, S. (2015). A new hvdc grid test system for hvdc grid dynamics and protection studies in emt-type software. *International Conference on AC and DC Power Transmission*.
- Machowski, J., Lubosny, Z., Bialek, J.W., and Bumby, J.R. (2020). *Power System Dynamics: Stability and Control*. John Wiley, Hoboken, NJ, USA, 3 edition.
- Martinez-Rodrigo, F., Ramirez, D., Rey-Boue, A.B., de Pablo, S., and de Lucas, L.C.H. (2017). Modular multilevel converters: Control and applications. *Energies*, 10.
- Pfeiffer, M., Hedtke, S., and Franck, C.M. (2018). Corona current coupling in bipolar hvdc and hybrid hvac/hvdc overhead lines. *IEEE Transactions on Power Delivery*, 33(1), 393 – 402.
- Rekik, A., Boukettaya, G., and Kallel, R. (2018). Comparative study of two control strategies of a multiterminal vsc-hvdc systems. *7th International Conference on Systems and Control*.
- Sanchez, S., Garces, A., Bergna, G., and Tedeschi, E. (2019). Dynamics and stability of meshed multiterminal hvdc networks. *IEEE Transactions on Power Delivery*, 34(3), 1824 – 1833.
- Santos, M.S. and Barros, L.S. (2019). Offshore wind energy conversion system based on squirrel cage induction generator connected to the grid by vsc-hvdc link. *IEEE PES Innovative Smart Grid Technologies Conference - Latin America*.
- Santos, M.S., Barros, L.S., Costa, F.B., Barros, C.M.V., Junior, G.P.S., and Strunz, K. (2022a). Frequency droop-based synchronverter without battery for primary support of microgrids. *Journal of Control, Automation and Electrical Systems*.
- Santos, M.S., Barros, L.S., França, R.L.S., Costa, F.B., and Strunz, K. (2022b). A meshed mmc-based mtdc system with improved voltage margin control for robustness towards disturbances. *Journal of Control, Automation and Electrical Systems*.
- Ye, H., Gao, S., Li, G., and Liu, Y. (2021). Efficient estimation and characteristic analysis of short-circuit currents for mmc-mtdc grids. *IEEE Transactions on Industrial Electronics*, 68(1), 258–269.